

Static impurity in a mesoscopic system of $SU(N)$ fermionic matter-waves

Juan Polo,¹ Wayne J. Chetcuti,¹ Anna Minguzzi,² Andreas Osterloh,¹ and Luigi Amico^{1,3,4}

¹Quantum Research Center, Technology Innovation Institute, Abu Dhabi 9639, UAE

²Université Grenoble Alpes, CNRS, LPMMC, 38000 Grenoble, France

³Dipartimento di Fisica e Astronomia “Ettore Majorana” University of Catania, Via S. Sofia 64, 95123 Catania, Italy

⁴INFN-Sezione di Catania, Via S. Sofia 64, 95123 Catania, Italy

(Dated: November 25, 2024)

We investigate the effects of a static impurity, modeled by a localized barrier, in a one-dimensional mesoscopic system comprised of strongly correlated repulsive $SU(N)$ -symmetric fermions. For a mesoscopic sized ring under the effect of an artificial gauge field, we analyze the particle density and the current flowing through the impurity at varying interaction strength, barrier height and number of components. We find a non-monotonic behaviour of the persistent current, due to the competition between the screening of the impurity, quantum fluctuations, and the phenomenon of fractionalization, a signature trait of $SU(N)$ fermionic matter-waves in mesoscopic ring potentials. This is also highlighted in the particle density at the impurity site. We show that the impurity opens a gap in the energy spectrum selectively, constrained by the total effective spin and interaction. Our findings hold significance for the fundamental understanding of the localized impurity problem and its potential applications for sensing and interferometry in quantum technology.

Introduction – The interplay between localized impurities and correlations in quantum many-body systems is an important topic for both basic and applied physical science, ranging from mesoscopic physics [1] and nano-electronics [2] to high- T_c superconductivity [3] and spin liquids [4]. In this regard, Kane and Fisher carried out a groundbreaking work where they investigated an interacting electronic system at low energy, and confined in an infinitely long wire interrupted by a single localized barrier [5, 6]. Focusing on repulsively interacting particles, even arbitrary small barriers were found to tend to infinity (under renormalization group flow). Such remarkable results triggered a series of studies that shed light on different aspects of strongly correlated matter [4, 7–10].

The emergence of quantum technology has ushered in a new stage of addressing impurity problems, marked by the ability to manipulate systems on a fundamental level using newly engineered physical platforms such as cold atoms and superconducting networks. This unprecedented control enables the exploration of such systems in the presence of impurities with remarkable flexibility and precision over relevant parameters, including the characteristics of barriers and the nature of particle correlations [11–16]. Concurrently, novel applications have arisen, leveraging the interplay between impurity and correlations to craft quantum devices with enhanced performances, spanning from Josephson junction-based devices [17–23] to rotation sensors [24, 25], and interferometers wherein the static impurity can serve as a matter-wave beam splitter [26–29].

Our study focuses on a localized impurity in a one-dimensional mesoscopic system of N -component fermions, which are particles with N internal degrees of freedom that can be treated as an effective spin. On increasing the number of components, the Pauli exclusion principle relaxes allowing N particles to occupy the same quantum state, with interactions effects expected to be enhanced, leading to novel and interesting physics [30].

We note that as $N \rightarrow \infty$, keeping the number of particles $N_p < N$, provides a “bosonic” limit [31].

Specifically, we consider $SU(N)$ symmetric fermions with component independent repulsive interactions [32–34]. Besides other approaches [5–10], the problem can be investigated through persistent currents flowing in annular matter-wave circuits pierced by an effective magnetic field. The latter has been pursued in circuits of spinless bosons [21, 35, 36]. Though, the spin degrees of freedom provide a significant complexity in impurity physics. When confined in mesoscopic ring-shaped potentials, at strong interactions $SU(N)$ fermions sustain persistent currents with fractional flux quanta ϕ_0/N_p , with ϕ_0 being the bare flux quantum of the free fermion case [37, 38]. This phenomenon of fractionalization reflects the formation of a collective state in which particles are arranged in the ring with a high stiffness conferred by spin correlations. We refer to the latter as ‘ring droplet’. Such behaviour, coupled with the knowledge that spin correlations and symmetries are known to play a crucial role in impurity problems [39], provides a compelling motivation for our study. In addition, $SU(N)$ fermions are experimentally realizable with alkaline earth-like cold atoms [30, 40–44]. A recent study has proposed a protocol to experimentally realize $SU(N)$ -symmetric systems through shielded ultracold molecules, which would circumvent the limitations of lack of tunable interactions through Feshbach resonances and different particle statistics [45, 46].

In this paper, we show that the underlying physics of $SU(N)$ matter-waves flowing through a barrier is characterized by the interplay between its strength and the particle interaction, with the number of components setting a further dimension in the parameter space of the problem. Specifically, the influence of the single localized impurity, its enhancement or screening, strongly hinges on this contention as evidenced by our study of the spatial density. Remarkably, we also find a non-monotonic

behaviour of the current amplitude for fixed impurity strength with increasing interaction, which reflects the competition between the single-particle quantum dynamics, and collective effects implied by the ring droplet formation in conjunction with the quantum phase fluctuations arising from the particles' strong interaction. In our analysis, we employ a combination of numerical methods (exact diagonalization) and analytical techniques (Bethe ansatz) when applicable.

SU(N) fermionic matter-wave currents – Consider N_p strongly interacting N -component fermions of mass m residing on a mesoscopic one-dimensional ring-shaped optical lattice composed of N_s sites threaded by an effective magnetic flux ϕ . The ring contains an impurity in the form of a localized potential barrier, breaking the discrete translational invariance. Such a scenario can be modeled through the multi-component Fermi-Hubbard Hamiltonian [33, 34]

$$\mathcal{H} = \sum_{j=1}^{N_s} \left[-t \sum_{\alpha}^N (e^{i\Omega} c_{j,\alpha}^{\dagger} c_{j+1,\alpha} + e^{-i\Omega} c_{j+1,\alpha}^{\dagger} c_{j,\alpha}) + \sum_{\alpha \neq \beta}^N U_{\alpha\beta} n_{j,\alpha} n_{j,\beta} + \sum_{\alpha}^N \lambda_{j,\alpha} n_{j,\alpha} \right], \quad (1)$$

where $c_{j,\alpha}^{\dagger}$ ($c_{j,\alpha}$) creates (destroys) a fermion with colour α on site j and $n_{j,\alpha} = c_{j,\alpha}^{\dagger} c_{j,\alpha}$ is the local number operator. The parameters t and U correspond to the hopping and on-site interaction energies respectively. Unless explicitly stated, we adopt isotropic interactions $U_{\alpha\beta} = U$, turning Eq. (1) into the SU(N) Hubbard model. In this case: (i) it is a model that well represents experimentally realizable lattices of alkaline earth-like cold atoms [33, 42]; (ii) the system is, for $\lambda_{\alpha} = 0$, Bethe Ansatz integrable in the continuous limit of vanishing lattice spacing as it tends to the Gaudin-Yang-Sutherland model [47] (see App. I). The barrier of strength λ is equal for all colours localized at site j_0 such that $\lambda_{j,\alpha} = \lambda \delta_{j,j_0}$, taken to be positive. All energies will be given in units of t .

The artificial gauge field $\Omega = (2\pi\phi)/(N_s\phi_0)$ is introduced through the Peierls substitution $t \rightarrow te^{i\Omega}$ [48]. For neutral cold atoms, the synthetic field can be introduced through various means [49], resulting in a Hamiltonian of the same form as that in Eq. (1) albeit with a different parametric expression for the elementary flux quantum ϕ_0 , which encodes the physical nature of the specific implementation. One instance is that of inducing rotation through stirring [50, 51], which is particularly suitable in the presence of a barrier, where $\phi_0 = \hbar/(mR^2)$ with R being the radius of the ring (taken to be equal to 1 in our case). In the presence of a flux, the many-body spectrum in the free particle regime is piece-wise parabolic, caused by energy level crossings between parabolas of well-defined angular momentum per particle, denoted by ℓ , to counteract the increase in flux piercing the system. Consequently, the energy spectrum is periodic in ϕ with

a period fixed by ϕ_0 akin to that of particles in a periodic potential. Therefore, following Leggett, $E(\phi)$ define the ‘Bloch bands’ of the problem in which the magnetic flux plays the role of the momentum [52].

In order to characterize the flow of SU(N) fermionic particles through a localized barrier, we utilize the spatial density $\langle n_j \rangle$ and the persistent current $I(\phi)$, which is the system's response to the applied field ϕ . At zero temperature, the persistent current is obtained from the ground-state energy E_0 : by the relation $I(\phi) = -\partial E_0/\partial\phi$. We employ the Hellmann-Feynmann theorem to calculate the species-wise current $I_{\alpha}(\phi)$, which for lattice systems, reads $I_{\alpha}(\phi) = -(2t\pi)/(\phi_0 N_s) \sum_{j=1}^{N_s} \langle e^{i\Omega} c_{j,\alpha}^{\dagger} c_{j+1,\alpha} - \text{h.c.} \rangle_{GS}$ with $\langle \bullet \rangle_{GS}$ being the ground-state expectation value. The resulting persistent current profile is a saw-tooth shape with the jumps corresponding to changes in the system's angular momentum due to level crossings. In cold atoms implementations, the saw-tooth character of the current gives rise to the discrete steps in the angular momentum per particle as observed in experiments [51].

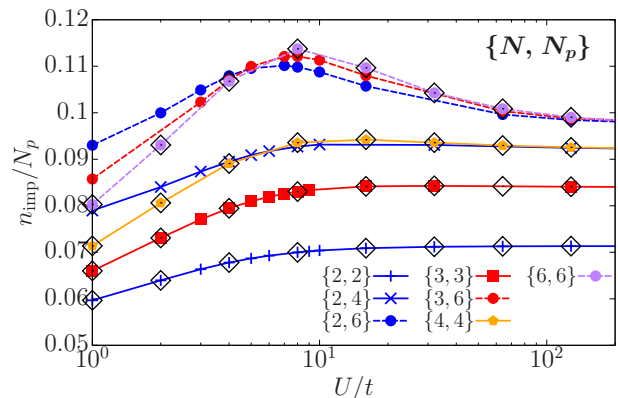


FIG. 1. Density at the impurity site n_{imp} versus interaction U/t for a fixed barrier strength λ/t with different particles N_p and components N . For systems with odd N_p/N , results are shown for flux value $\phi = 0$; systems with even N_p/N are taken at $\phi/\phi_0 = 0.5$ due to a parity effect (see App. III). Grey triangles correspond to bosons with same N_p . Results obtained with exact diagonalization of the SU(N) Hubbard and Bose-Hubbard models for $N_s = 7$ sites.

Fermionic matter-wave currents, without an impurity, in the strongly interacting regime exhibit a reduced periodicity depending on the nature of interactions the particles are subjected to. For repulsive interactions results in N_p piece-wise parabolic segments per flux quantum [37] (see [53] for attractive case). The reduced periodicity of the current reflects a fractional flux quantum ϕ_0/N_p mediated by energy level crossings at $n\phi_0/(2N_p)$ for odd integer n . The phenomenon of fractionalization is specific to a mesoscopic system with periodic boundary conditions reflecting a collective state (ring droplet) that results in a stiff particle arrangement due to spin correlations [37].

Screening of the local impurity – Monitoring the spatial profile of the particle density gives valuable insight into the impact of the impurity on the system. Due to the barrier’s presence, there is a global minimum in the density at the site where it is located, denoted by n_{imp} . For free fermions and no flux, the dip in n_{imp} can be straightforwardly understood from Eq. (1), as the particles will tend to avoid the barrier to minimize $E(\phi)$. The reduction in n_{imp} with decreasing N_p/N reflects the loosening of the Pauli principle for large N enabling more particles to reside at the impurity site enhancing its effect (see App. III). By fixing λ and switching on U , n_{imp} displays a monotonous increasing behaviour as the barrier’s effect dwindles for stronger interactions – Fig. 1. Essentially, the increased repulsion between the particles, which is more pronounced for larger N , screens the barrier, i.e. n_{imp} grows. As $U \rightarrow \infty$, n_{imp} saturates to a constant value disregarding the distinction between various N , coinciding with that of hard-core bosons/spinless fermions, due to the formation of the aforementioned ‘ring droplet’ of N_p particles.

When N_s is comparable to N_p , the density at the barrier is non-monotonous with increasing U – Fig. 1. For weak U , the rate at which the barrier is screened is larger with increasing N , and further dictated by N_p (see App. III) [54]. On account of this rate dependence, the trend observed for free fermions, impurity being more effective with decreasing N_p/N , is reversed at intermediate U . For large but finite interactions, particles tend to dwell in the barrier as it acts as a shield against the strong repulsion, with a similar rate as mentioned previously.

Persistent current through a localized barrier – The interplay between the impurity strength and interaction manifests itself in the persistent current profile. Focusing on the current’s maximum amplitude I_{max} , we find that it exhibits a non-monotonous behaviour as a function of λ and U – Fig. 2. Despite the qualitative similarities compared to repulsive bosons [35], the underlying mechanisms are much more subtle due to the effective spin degrees of freedom. Specifically, such behaviour arises because of the competition between the single-particle quantum dynamics (screening), and a collective one resulting from a combination of quantum phase fluctuations and the fractionalization stemming from the ring droplet state.

For free particles, the presence of the impurity reduces I_{max} , as one can intuitively expect – Fig. 2. Essentially, the role of the barrier is to diminish the matter-wave flow. Furthermore, it opens a gap at all the degeneracy points in the Bloch band $E_0(\phi)$, reflected by the smearing out of the characteristic saw-tooth shape of the current.

Keeping the barrier strength fixed and going to weak interactions, the current amplitude increases at a rate favouring N in accordance with the impurity screening observed in the density – Fig. 2. The trend of the impurity’s influence with N in the density and current appear to go against each other. However, this is because for a given N_p the current is greater for larger N . Typi-

cally, in the absence of an impurity, I_{max} is monotonically decreasing with U because of partial fractionalization. However, for $\lambda > 0$, such an effect is suppressed and does not exert its influence immediately on the system. Indeed, for $N_p/N = 1$, where the Pauli principle is absent, the current overlaps the bosonic one in this regime, hence corroborating the picture. For intermediate interactions such that $U/\lambda > 1$, where the phenomenon of fractionalization becomes more pronounced, the current undergoes a ‘hybridization’ becoming a smoothed yet fractionalized one with cusps, exhibiting a reduced periodicity (see App. IV). Subsequently, I_{max} emerges from the cusped parabolas – Fig. 3. We point out that in this regime, the behaviour of I_{max} deviates from bosons since fractionalization is not present in the latter [51].

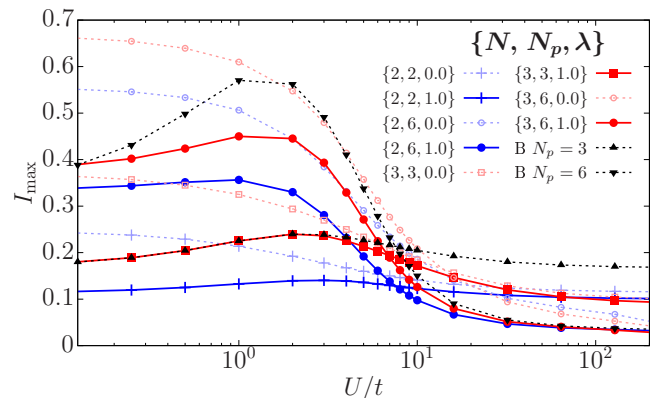


FIG. 2. Maximum persistent current amplitude I_{max} as a function of interaction U/t in the presence of a barrier with strength λ/t for different number of particles N_p and components N (solid lines). The black dotted lines correspond to a system of bosons with a given N_p , whilst the other dotted lines correspond to I_{max} with no barrier. Results obtained with exact diagonalization of the $SU(N)$ Hubbard and Bose-Hubbard models for $N_s = 7$ sites.

In the limit of strong interactions, as $U/\lambda \gg 1$, the impact of the impurity is drastically reduced. Nonetheless, we find that the current is strongly suppressed. Such an effect primarily originates from the fractionalization whose rate is enhanced with N [37]. Correspondingly, the persistent current displays a perfect saw-tooth shape with a reduced periodicity of $1/N_p$ exhibiting negligible signs of smearing. Naturally, this result is to be expected since in the absence of a barrier I_{max} decays, eventually saturating to a constant value found through Bethe Ansatz, as a consequence of the fractionalization [37]. Such behaviour is also present for repulsive bosons where this phenomenon emerges solely from the interplay between interactions and phase fluctuations [35].

Besides capturing the screening effect, a flux-dependent density emerges when an impurity is present providing insight into matter-wave flow. Specifically, in Fig. 3(b) the density profile reflects the reduced periodicity of the energy and current landscape. As the circulating current increases (decreases), the barrier’s ef-

fectiveness is enhanced (reduced) to counterbalance the particle flow. Accordingly, the density minimum is found to be encapsulating the current's periodic nature with ϕ . Consequently, the measurement of the particles' density could be used to monitor fractionalization as an alternative method to the interference dynamics [55].

Analysis of the spectral gap – The presence of an impurity in a single-component quantum system, including bosons with repulsive or attractive interactions, is known to split *all* the degeneracies in $E_0(\phi)$ to open a spectral gap Δ [21, 35, 36, 51]. At these avoided crossings, a coherent superposition of different angular momentum states is created. Consequently, the persistent current's saw-tooth shape starts to smoothen out at weak barriers, eventually becoming a sinusoid as λ gets large enough.

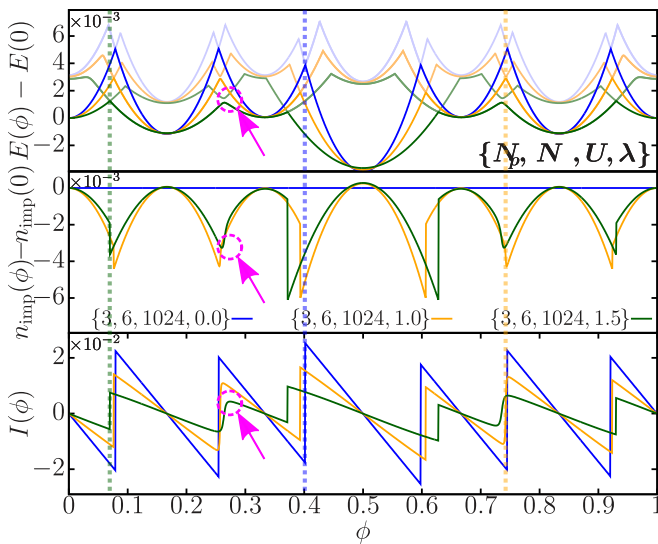


FIG. 3. Profiles of the energy $E(\phi)$ (top), corresponding density at the impurity site n_{imp} (middle) and the persistent current $I(\phi)$ (bottom) against the effective magnetic flux ϕ in the regime of strong interactions $U/t = 1024$ for various barrier strengths λ/t in a ring of N_s sites. Dotted lines highlight the correspondence of the current maxima and density minima, whilst circles indicate the opening of the gap in $E(\phi)$ and corresponding changes in n_{imp} and $I(\phi)$. The Casimir values s for each energy parabola are $\{6, 3, 3, 0, 3, 3, 6\}$. Results obtained with exact diagonalization of the $SU(N)$ Hubbard model with $N_s = 7$ sites.

For the present case of interacting $SU(N)$ fermions, only specific degeneracies in $E_0(\phi)$ are found to be split. The mechanism behind these selective gap openings lies in the internal degrees of freedom [56]. Indeed, as the barrier in Eq. (1) commutes with the quadratic $SU(N)$ Casimir operators with eigenvalue s , which characterizes each piece-wise parabola of the energy landscape (see App. V; [57, 58]), it is unable to couple states with different values of s [59]. In turn, the Bloch bands and the corresponding persistent current landscape are found to display a non-trivial dependence on s . Specifically, depending on N_p and N , the ground and excited states intersect each other as U increases: N_p dictates the amount

of energy level crossings and as such the fractionalization; N governs the quantity and ϕ dependence of the gaps through the $SU(N)$ Casimir. Such behaviour leads to a ground-state exhibiting a specific piece-wise dependence on s . Consequently, only crossings characterized by the same Casimir value can be split by the barrier to generate a gap – Fig. 3. Note that breaking the $SU(N)$ symmetry explicitly by adopting anisotropic interactions as in Eq. (1) or through a species selective barrier generates more gaps at the degeneracy points of $E_0(\phi)$ (see App. V).

Analysis of the spectral gap provides additional insight into the problem. For weak barriers, we find that Δ scales as λ/U (see App. V), which is corroborated by the closing of the gaps at all degeneracy points for strong interactions. Such scaling behaviour can be understood by considering the Bethe Ansatz equations as $U \rightarrow \infty$ [57, 60]. In this regime, the dependence of Δ on interaction traces back from the t^2/U scaling of the energy contribution of the spin part (see [37]). This can be seen from the commutator of the interaction term of model (1) and the barrier, which tends to zero, as the impurity only affects the tight-binding part of the model. For the case of stronger barriers, we find that the gap scales non-linearly with λ , as $\Delta(U, \lambda) \approx \frac{\lambda^\gamma}{U}$ with $\gamma > 1$ outside the linear response behaviour expected at low λ .

Discussions and Conclusions – The physics of a single localized impurity in a one-dimensional mesoscopic system of repulsive $SU(N)$ fermions subjected to an artificial gauge field is examined through the spatial density and the matter-wave flow. Besides the already intricate competition between interaction U , barrier strength λ and mesoscopic size, the problem acquires a new facet shaped by the N components.

Through analysis of the density at the impurity site against interaction, we find that the barrier is screened with a rate dependence that becomes larger with N . The maximum rate is achieved at $N_p/N = 1$ as the system effectively tends to a “bosonic” limit. As more particles can reside at the impurity site, the impurity is screened faster since the effective repulsion is enhanced as NU in $SU(N)$ systems. As $U \rightarrow \infty$, the density is found to saturate to a value that is independent of N because of the formation of the ring droplet with a stiff particle arrangement[38]. The density's behaviour at the barrier in these two regimes portrays the interplay between single-particle and collective dynamics.

Our other probe, the persistent current, being a flow of matter, sheds further light on this competition. Indeed, the current amplitude I_{max} exhibits a non-monotonic behaviour as a function of the interactions that, albeit qualitatively similar to bosons, is underpinned by substantially different machinery. Whilst at weak U , I_{max} increases due to the suppression of impurity as observed in the density, this is not the case on going to stronger interactions. The amplitude decreases as a combined effect of quantum phase fluctuations, which can trigger phase slips

across the impurity, and fractionalization arising from spin correlations on setting the ring droplet in motion. The latter phenomenon is absent for bosons, accounting for the deviation between their current and that of fermions with $N_p/N = 1$. An additional important difference is that for $SU(N)$ fermions, gaps open only at energy level crossings having the same total effective spin s measured by the quadratic $SU(N)$ Casimir since the barrier cannot couple different spin sectors. For a given N_p , the number and the location of the gap openings is thus dictated by N .

The study of $SU(N)$ fermions confined in rings poses an interesting challenge both from an analytical and numerical standpoint. Analytical techniques have been found at strong interactions [57] while numerically ones face the known problems coming from the periodic boundary conditions (DMRG) combined with a high degeneracy in the ground state. To address these limits, further develop-

ment are being explored [61, 62].

We remark that our study is in a very different regime in which the standard one-dimensional Luttinger theory can be applied since the Fermi sphere in our system is hardly filled [9]. Moreover, as we discussed above, the physics is significantly affected by the coupling between spin and charge degrees of freedom. Finding an appropriate effective renormalization group description [63] of the problem would be a necessary step forward.

To conclude, we highlight that static impurities are of high relevance for quantum technology, and in particular for quantum sensing [29, 36, 49, 64–66]. Therefore, the setup considered here can also provide the basis for current-based devices and interferometers utilizing N -component matter-waves.

Acknowledgements – We thank Enrico C. Domanti and Sam Carr for useful discussions.

-
- [1] B. L. Altshuler, P. A. Lee, and W. R. Webb, *Mesoscopic phenomena in solids* (Elsevier, 2012).
- [2] G. L. Timp and R. E. Howard, *IEEE Proc.* **79**, 1188 (1991).
- [3] H. Alloul, J. Bobroff, M. Gabay, and P. Hirschfeld, *Rev. Mod. Phys.* **81**, 45 (2009).
- [4] A. Kolezhuk, S. Sachdev, R. R. Biswas, and P. Chen, *Phys. Rev. B* **74**, 165114 (2006).
- [5] C. Kane and M. P. Fisher, *Phys. Rev. Lett.* **68**, 1220 (1992).
- [6] C. Kane and M. P. Fisher, *Physical Review B* **46**, 15233 (1992).
- [7] J. Von Delft and H. Schoeller, *Annalen der Physik* **510**, 225 (1998).
- [8] H. Saleur, in *Topological aspects of low dimensional systems: Session LXIX* (Springer, 2002) p. 473.
- [9] T. Giamarchi, *Quantum physics in one dimension*, Vol. 121 (Clarendon Press, 2003).
- [10] C. Rylands and N. Andrei, *Phys. Rev. B* **94**, 115142 (2016).
- [11] P. Manju, K. Hardman, M. Sooriyabandara, P. Wigley, J. Close, N. Robins, M. Hush, and S. Szigeti, *Physical Review A* **98**, 053629 (2018).
- [12] S. Léger, J. Puertas-Martínez, K. Bharadwaj, R. Dassonneville, J. Delaforce, F. Foroughi, V. Milchakov, L. Planat, O. Buisson, C. Naud, *et al.*, *Nat. Comm.* **10**, 5259 (2019).
- [13] J. Puertas Martínez, S. Léger, N. Gheeraert, R. Dassonneville, L. Planat, F. Foroughi, Y. Krupko, O. Buisson, C. Naud, W. Hasch-Guichard, S. Florense, I. Snyman, and N. Roch, *New Phys. J. Q. Inf.* **5**, 19 (2019).
- [14] R. Kuzmin, N. Grabon, N. Mehta, A. Burshtein, M. Goldstein, M. Houzet, L. I. Glazman, and V. E. Manucharyan, *Phys. Rev. Lett.* **126**, 197701 (2021).
- [15] S. Mistakidis and A. Volosniev, *Physics of Impurities in Quantum Gases* (MDPI, 2022).
- [16] S. Léger, T. Sépulcre, D. Fraudet, O. Buisson, C. Naud, W. Hasch-Guichard, S. Florens, I. Snyman, D. M. Basko, and N. Roch, *SciPost Phys.* **14**, 130 (2023).
- [17] M. Nadeem, M. S. Fuhrer, and X. Wang, *Nature Rev. Phys.* **5**, 558 (2023).
- [18] A. Hriscu and Y. V. Nazarov, *Phys. Rev. B* **83**, 174511 (2011).
- [19] M. Trahms, L. Melischek, J. F. Steiner, B. Mahendru, I. Tamir, N. Bogdanoff, O. Peters, G. Reecht, C. B. Winkelmann, F. von Oppen, *et al.*, *Nature* **615**, 628 (2023).
- [20] C. Ryu, P. W. Blackburn, A. A. Blinova, and M. G. Boshier, *Phys. Rev. Lett.* **111**, 205301 (2013).
- [21] D. Aghamalyan, M. Cominotti, M. Rizzi, D. Rossini, F. Hekking, A. Minguzzi, L.-C. Kwek, and L. Amico, *New J. Phys.* **17**, 045023 (2015).
- [22] G. Valtolina, A. Burchianti, A. Amico, E. Neri, K. Khani, J. A. Seman, A. Trombettoni, A. Smerzi, M. Zaccanti, M. Inguscio, and G. Roati, *Science* **350**, 1505 (2015).
- [23] V. P. Singh, J. Polo, L. Mathey, and L. Amico, *Physical Review Letters* **133**, 093401 (2024).
- [24] C. Ryu, E. C. Samson, and M. G. Boshier, *Nat. Comm.* **11** (2020), 10.1038/s41467-020-17185-6.
- [25] O. Adeniji, C. Henry, S. Thomas, R. C. Sapp, A. Goyal, C. W. Clark, and M. Edwards, “Double-target BEC atomtronic rotation sensor,” (2024), arXiv:2411.06585 [cond-mat.quant-gas].
- [26] R. Godun, M. d’Arcy, G. Summy, and K. Burnett, *Contemp. Phys.* **42**, 77 (2001).
- [27] S. A. Haine, *New J. Phys.* **20**, 033009 (2018).
- [28] O. J. Wales, A. Rakonjac, T. P. Billam, J. L. Helm, S. A. Gardiner, and S. L. Cornish, *Communications Physics* **3**, 51 (2020).
- [29] P. Naldesi, J. Polo, P. D. Drummond, V. Dunjko, L. Amico, A. Minguzzi, and M. Olshanii, *SciPost Physics* **15**, 187 (2023).
- [30] L. Sonderhouse, C. Sanner, R. B. Hutson, A. Goban, T. Bilitewski, L. Yan, W. R. Milner, A. M. Rey, and J. Ye, *Nature Physics* **16**, 1216 (2020).
- [31] H. Frahm and A. Schadschneider, “On the bethe ansatz soluble degenerate hubbard model,” in *The Hubbard Model: Its Physics and Mathematical Physics*, edited by D. Baeriswyl, D. K. Campbell, J. M. P. Carmelo, F. Guinea, and E. Louis (Springer US, Boston, MA,

- 1995) p. 21.
- [32] A. V. Gorshkov, M. Hermele, V. Gurarie, C. Xu, P. S. Julienne, J. Ye, P. Zoller, E. Demler, M. D. Lukin, and A. M. Rey, *Nature Physics* **6**, 289 (2010).
- [33] M. A. Cazalilla and A. M. Rey, *Reports on Progress in Physics* **77**, 124401 (2014).
- [34] S. Capponi, P. Lecheminant, and K. Totsuka, *Annals of Physics* **367**, 50 (2016).
- [35] M. Cominotti, D. Rossini, M. Rizzi, F. Hekking, and A. Minguzzi, *Phys. Rev. Lett.* **113**, 025301 (2014).
- [36] J. Polo, P. Naldesi, A. Minguzzi, and L. Amico, *Q. Sci. Tech.* **7**, 015015 (2021).
- [37] W. J. Chetcuti, T. Haug, L.-C. Kwek, and L. Amico, *SciPost Physics* **12**, 33 (2022).
- [38] W. J. Chetcuti, *Persistent Currents in Atomtronic Circuits of $SU(N)$ Fermions*, Ph.D. thesis, University of Catania (2023), 2311.03072.
- [39] N. Andrei, K. Furuya, and J. H. Lowenstein, *Reviews of Modern Physics* **55**, 331 (1983).
- [40] S. Taie, R. Yamazaki, S. Sugawa, and Y. Takahashi, *Nature Physics* **8**, 825 (2012).
- [41] G. Pagano, M. Mancini, G. Cappellini, P. Lombardi, F. Schäfer, H. Hu, X.-J. Liu, J. Catani, C. Sias, M. Inguscio, and L. Fallani, *Nature Physics* **10**, 198 (2014).
- [42] F. Scazza, C. Hofrichter, M. Höfer, P. De Groot, I. Bloch, and S. Fölling, *Nature Physics* **10**, 779 (2014).
- [43] C. Hofrichter, L. Riegger, F. Scazza, M. Höfer, D. R. Fernandes, I. Bloch, and S. Fölling, *Phys. Rev. X* **6**, 021030 (2016).
- [44] S. Taie, E. Ibarra-García-Padilla, N. Nishizawa, Y. Takasu, Y. Kuno, H.-T. Wei, R. T. Scalettar, K. R. A. Hazzard, and Y. Takahashi, *Nature Physics* (2022), 10.1038/s41567-022-01725-6.
- [45] B. Mukherjee, J. M. Hutson, and K. R. A. Hazzard, “ $SU(N)$ magnetism with ultracold molecules,” (2024), arXiv:2404.15957 [cond-mat.quant-gas].
- [46] B. Mukherjee and J. M. Hutson, “ $SU(N)$ symmetry with ultracold alkali dimers: weak dependence of scattering properties on hyperfine state,” (2024), arXiv:2410.19068 [quant-ph].
- [47] B. Sutherland, *Phys. Rev. Lett.* **20**, 98 (1968).
- [48] R. Peierls, *Zeitschrift für Physik* **80**, 763 (1933).
- [49] L. Amico, M. Boshier, G. Birkel, A. Minguzzi, C. Miniatura, L.-C. Kwek, D. Aghamalyan, V. Ahufinger, D. Anderson, and e. a. Andrei, *AVS Q. Sci.* **3**, 039201 (2021).
- [50] K. C. Wright, R. B. Blakestad, C. J. Lobb, W. D. Phillips, and G. K. Campbell, *Physical Review Letters* **110**, 025302 (2013).
- [51] J. Polo, W. J. Chetcuti, T. Haug, A. Minguzzi, K. Wright, and L. Amico, “Persistent currents in ultracold gases,” (2024), arXiv:2410.17318 [cond-mat.quant-gas].
- [52] A. J. Leggett, “Dephasing and Non-Dephasing Collisions in Nanostructures,” in *Granular Nanoelectronics* (Springer US, Boston, MA, 1991) p. 297.
- [53] W. J. Chetcuti, J. Polo, A. Osterloh, P. Castorina, and L. Amico, *Comm. Phys.* **6** (2023), 10.1038/s42005-023-01256-3.
- [54] The barrier is the least effective versus interactions at $N_p = N$. In this case, the density at the impurity site coincides with that of a bosonic system of the same N_p . Such a behaviour reflects the lack of a meaningful Pauli exclusion principle in the system.
- [55] W. J. Chetcuti, A. Osterloh, L. Amico, and J. Polo, *SciPost Phys.* **15**, 181 (2023).
- [56] On account of this, such behaviour is different than that of bosons, even the ones with attractive interactions where fractionalization is present.
- [57] A. Osterloh, J. Polo, W. J. Chetcuti, and L. Amico, *SciPost Physics* **15**, 006 (2023).
- [58] G. Pecci, G. Aupetit-Diallo, M. Albert, P. Vignolo, and A. Minguzzi, *Comptes Rendus Physique* **24**, 1 (2023).
- [59] Note that the $SU(N)$ representation can be different, which would generally be indicated by a different s . However, for some N the different representations can share the same s .
- [60] M. Ogata and H. Shiba, *Physical Review B* **41**, 2326 (1990).
- [61] T. Botzung and P. Nataf, *Phys. Rev. Lett.* **132**, 153001 (2024).
- [62] A. Weichselbaum, “Qspace - an open-source tensor library for abelian and non-abelian symmetries,” (2024), arXiv:2405.06632 [cond-mat.str-el].
- [63] A. O. Gogolin, A. A. Nersisyan, and A. M. Tsvelik, *Bosonization and strongly correlated systems* (Cambridge university press, 2004).
- [64] L. Amico, D. Anderson, M. Boshier, J.-P. Brantut, L.-C. Kwek, A. Minguzzi, and W. von Klitzing, *Reviews of Modern Physics* **94**, 041001 (2022).
- [65] J. Polo, W. J. Chetcuti, E. C. Domanti, P. Kitson, A. Osterloh, F. Percivalle, V. P. Singh, and L. Amico, *Q. Sci. Tech.* **9**, 030501 (2024).
- [66] P. Naldesi, J. Polo, V. Dunjko, H. Perrin, M. Olshanii, L. Amico, and A. Minguzzi, *SciPost Physics* **12**, 138 (2022).
- [67] D. Schmeltzer and R. Berkovits, *Physics Letters A* **253**, 341 (1999).
- [68] F. H. L. Essler, H. Frahm, F. Göhmann, A. Klümper, and V. E. Korepin, *The One-Dimensional Hubbard Model* (Cambridge University Press, 2005).
- [69] B. Sutherland, *Physical Review B* **12**, 3795 (1975).
- [70] N. Yu and M. Fowler, *Physical Review B* **45**, 11795 (1992).
- [71] Holds when the charge quantum numbers are consecutive integers/half-odd integers as is always the case with the ground-state.
- [72] M. Consiglio, W. J. Chetcuti, C. Bravo-Prieto, S. Ramos-Calderer, A. Minguzzi, J. I. Latorre, L. Amico, and T. J. G. Apollaro, *J. Phys. A* **55**, 265301 (2022).
- [73] S. D. Huber, B. Theiler, E. Altman, and G. Blatter, *Phys. Rev. Lett.* **100**, 050404 (2008).
- [74] It happens that for certain groups there are doubly (or multiply) occurring values for the Casimir, which belong to different representations. Here, it is of importance whether the states belong to the same representation or not. The Casimir value serves to label these representations.
- [75] Diamagnetic/paramagnetic parity with even N and paramagnetic parity with odd N .

In the following, we provide supporting details of the result found in the manuscript ‘*Static impurity in a mesoscopic system of $SU(N)$ fermions*’.

I. MAPPING BETWEEN THE GAUDIN-YANG-SUTHERLAND AND $SU(N)$ HUBBARD MODELS

Following the approach in [67], to sketch out the mapping between the lattice and continuous models we start by defining the density of N_p fermions in a ring of N_s sites with lattice spacing Δ as $D = N_p/(\Delta N_s)$. Subsequently, the filling fraction $\nu = N_p/N_s$ can be reformulated in terms of the lattice spacing $\nu = D\Delta$. As a result, in the continuous limit of vanishing lattice spacing, $\Delta \rightarrow 0$, and for finite particle density, the corresponding filling fraction must also be small. In order for the anti-commutation relations to be preserved in the continuous limit, one needs to re-scale the fermionic operators by the lattice spacing in the following manner

$$c_{j,\alpha}^\dagger = \sqrt{\Delta} \Psi_\alpha^\dagger(x_j) \quad n_{j,\alpha} = \Delta \Psi_\alpha^\dagger(x_j) \Psi_\alpha(x_j) \quad \text{where } x_j = j\Delta \quad (2)$$

with $\Psi_\alpha^\dagger(x_j)$ [$\Psi_\alpha(x_j)$] being the field operators that create (annihilate) a fermion with effective spin projection α at position x_j , obeying the standard anti-commutation relations $\{\Psi_\alpha(x), \Psi_\beta(y)\} = \delta_{\alpha,\beta} \delta(x-y)$ and $\{\Psi_\alpha^\dagger(x), \Psi_\beta^\dagger(y)\} = 0$. Plugging the re-scaled fermionic operators of Eq. (2) in the $SU(N)$ Hubbard model, we have that the Hamiltonian is mapped onto the Fermi gas quantum field theory \mathcal{H}_{FG} via $\mathcal{H}_{SU(N)} = t\Delta^2 \mathcal{H}_{FG} - 2N_p$ where

$$\mathcal{H}_{FG} = \int \left[-(\partial_x \Psi_\alpha^\dagger)(\partial_x \Psi_\alpha) + 2c \sum_{\alpha < \beta} \Psi_\alpha^\dagger \Psi_\beta^\dagger \Psi_\beta \Psi_\alpha \right] dx, \quad (3)$$

where α and β correspond to the different colours and we defined the interaction strength as $c = \frac{U}{4\Delta t}$ with t and U being the Hubbard model’s hopping and interaction strengths respectively. The eigenstates of \mathcal{H}_{FG} are of the given form

$$|\psi(\lambda)\rangle = \sum_{\alpha_1 \dots \alpha_{N_p}} \int \chi(\mathbf{x}|\lambda) \Psi_{\alpha_1}^\dagger(x_1) \dots \Psi_{\alpha_{N_p}}^\dagger(x_{N_p}) |0\rangle dx, \quad (4)$$

with $\chi(\mathbf{x}|\lambda)$ being eigenfunctions of the Gaudin-Yang-Sutherland model that reads

$$\mathcal{H}_{GYS} = -\frac{\hbar^2}{2m} \sum_{\alpha=1}^N \sum_{j=1}^{N_\alpha} \frac{\partial^2}{\partial x_{j,\alpha}^2} + 2c \sum_{\alpha < \beta} \sum_{j,k}^{N_p} \delta(x_{j,\alpha} - x_{k,\beta}), \quad (5)$$

where m denotes the mass of the particles and N_α is the number of particles per colour.

II. BETHE ANSATZ EQUATIONS OF THE GAUDIN-YANG-SUTHERLAND MODEL WITH TWISTED BOUNDARY CONDITIONS

In the presence of an effective magnetic flux ϕ , modifies the momentum of the fermions due to its coupling with the vector potential. Consequently, the Gaudin-Yang-Sutherland model of Eq. (5) can be re-written as

$$\mathcal{H}_{GYS} = -\frac{\hbar^2}{2m} \sum_{\alpha=1}^N \left[\sum_{j=1}^{N_\alpha} \left(\frac{\partial}{\partial x_{j,\alpha}} - \frac{2\pi}{L} \frac{\phi}{\phi_0} \right)^2 + 2c \sum_{\alpha < \beta} \sum_{j,k}^{N_p} \delta(x_{k,\alpha} - x_{j,\beta}), \right] \quad (6)$$

with ϕ_0 being the elementary flux quantum. The model is Bethe Ansatz integrable [47] through the following equations

$$e^{i(k_j L - 2\pi\phi)} = \prod_{\alpha=1}^{M_1} \frac{k_j - \Lambda_\alpha^{(1)} + i c}{k_j - \Lambda_\alpha^{(1)} - i c}, \quad j = 1, \dots, N_p \quad (7)$$

$$\prod_{\substack{\beta=1 \\ \beta \neq \alpha}}^{M_r} \frac{\Lambda_\alpha^{(r)} - \Lambda_\beta^{(r)} + 2i c}{\Lambda_\alpha^{(r)} - \Lambda_\beta^{(r)} - 2i c} = \prod_{\beta=1}^{M_{r-1}} \frac{\Lambda_\alpha^{(r)} - \Lambda_\beta^{(r-1)} + i c}{\Lambda_\alpha^{(r)} - \Lambda_\beta^{(r-1)} - i c} \cdot \prod_{\beta=1}^{M_{r+1}} \frac{\Lambda_\alpha^{(r)} - \Lambda_\beta^{(r+1)} + i c}{\Lambda_\alpha^{(r)} - \Lambda_\beta^{(r+1)} - i c}, \quad \alpha = 1, \dots, M_r \quad (8)$$

for $r = 1, \dots, N - 1$ where $M_0 = N_p$, $M_N = 0$ and $\lambda_\beta^{(0)} = k_\beta$. M_r corresponds to the number of spin rapidities per colour with k_j and $\Lambda_\alpha^{(r)}$ being the charge and spin momenta respectively. The energy of the system is given by $E = \sum_j^{N_p} k_j^2$. Let us take the SU(3) case as an example, wherein we have three non-linear equations,

$$e^{i(k_j L - \phi)} = \prod_{\alpha=1}^{M_1} \frac{k_j - \Lambda_\alpha + i c}{k_j - \Lambda_\alpha - i c} \quad j = 1, \dots, N_p, \quad (9)$$

$$\prod_{\beta \neq \alpha}^{M_1} \frac{\Lambda_\alpha - \Lambda_\beta + 2i c}{\Lambda_\alpha - \Lambda_\beta - 2i c} = \prod_{j=1}^{N_p} \frac{\Lambda_\alpha - k_j + i c}{\Lambda_\alpha - k_j - i c} \prod_{a=1}^{M_2} \frac{\Lambda_\alpha - \lambda_a + i c}{\Lambda_\alpha - \lambda_a - i c} \quad \alpha = 1, \dots, M_1, \quad (10)$$

$$\prod_{b \neq a}^{M_2} \frac{\lambda_a - \lambda_b + 2i c}{\lambda_a - \lambda_b - 2i c} = \prod_{\alpha=1}^{M_1} \frac{\lambda_a - \Lambda_\alpha + i c}{\lambda_a - \Lambda_\alpha - i c} \quad a = 1, \dots, M_2. \quad (11)$$

Note that for the sake of convenience, we changed $\Lambda_\alpha^{(1)}$ and $\Lambda_\alpha^{(2)}$ to Λ_α and λ_a . The first equation pertains to the charge quasimomenta with the other two accounting for the spin degrees of freedom, that emerge from the nested nature of the Bethe Ansatz. In the limit $\frac{U}{N_p} \rightarrow \infty$, we can neglect the terms k_j/U as they are much smaller in magnitude compared to the spin momenta and will tend to zero. As a result, the Bethe Ansatz equations simplify and are re-cast into the form

$$e^{i(k_j L - \phi)} = \prod_{\alpha=1}^{M_1} \frac{\Lambda_\alpha - i c}{\Lambda_\alpha + i c} \quad j = 1, \dots, N_p, \quad (12)$$

$$\prod_{\beta \neq \alpha}^{M_1} \frac{\Lambda_\alpha - \Lambda_\beta + 2i c}{\Lambda_\alpha - \Lambda_\beta - 2i c} = \left[\frac{\Lambda_\alpha + i c}{\Lambda_\alpha - i c} \right]^{N_p} \prod_{a=1}^{M_2} \frac{\Lambda_\alpha - \lambda_a + i c}{\Lambda_\alpha - \lambda_a - i c} \quad \alpha = 1, \dots, M_1, \quad (13)$$

$$\prod_{b \neq a}^{M_2} \frac{\lambda_a - \lambda_b + 2i c}{\lambda_a - \lambda_b - 2i c} = \prod_{\alpha=1}^{M_1} \frac{\lambda_a - \Lambda_\alpha + i c}{\lambda_a - \Lambda_\alpha - i c} \quad a = 1, \dots, M_2. \quad (14)$$

Essentially, there is a separation of the charge and spin degrees of freedom that decouples the rapidities in the Bethe Ansatz equations. Consequently, in this limit, the states Gaudin-Yang-Sutherland model can be written as a composition of the spinless model and SU(3) Heisenberg Hamiltonian [57, 60]. Indeed, Eqs. (13) and (14) correspond to the Bethe equations of the isotropic SU(3) Heisenberg chain barring a normalization constant [68].

Taking the logarithm of Eqs. (12) through (14) and utilizing the relation $2i \arctan x = \pm \pi + \ln \frac{x-i}{x+i}$, the quasimomenta k_j can be expressed [37] as

$$k_j L = 2\pi \left[I_j + \frac{1}{N_p} \left(\sum_{\alpha=1}^{M_1} J_\alpha + \sum_{a=1}^{M_2} L_a \right) + \phi \right], \quad (15)$$

with I_j and $\{J_\alpha, L_a\}$ being the quantum numbers parameterizing the Bethe equations, the first being associated with the charge quasimomenta and the others for the spin rapidities. Therefore, the energy of the system reads

$$E(\phi) = \left(\frac{2\pi}{L} \right)^2 \left[\sum_j^{N_p} I_j^2 + 2 \sum_j^{N_p} I_j \left(\frac{X}{N_p} + \phi \right) + N_p \left(\frac{X}{N_p} \right)^2 + N_p \left(2\phi \frac{X}{N_p} + \phi^2 \right) \right], \quad (16)$$

and consequently, the corresponding persistent current defined at zero temperature as $I(\phi) = -\partial E / \partial \phi$ acquires the following form in the regime of $U \rightarrow \infty$

$$I(\phi) = - \left(\frac{2\pi}{L} \right)^2 \left[2 \sum_j^{N_p} I_j + N_p \left(2 \frac{X}{N_p} + 2\phi \right) \right], \quad (17)$$

where $X = (\sum_{\alpha=1}^{M_1} J_{\alpha} + \sum_{a=1}^{M_2} L_a)$. For the general case of $SU(N)$ fermions, the expression for the persistent current is the same keeping in mind that $X = \sum_l^{N-1} \sum_{\alpha_l}^{M_l} J_{\beta_l}$ to account for the quantum numbers of the $N-1$ spin rapidities. Although the $SU(N)$ Hubbard model is not integrable, in the limit of infinite repulsion it is quite close to being to at least for the low-lying spectrum. Thus, by using the Bethe equations of the Lai-Sutherland model [69] corresponding to the $SU(N)$ Hubbard model with commensurate filling fractions, acquired by substituting $\lambda_{\beta}^{(0)} = \sin k_{\beta}$ and k_j with $\sin k_j$ in Eq. (7) due to lattice regularization [68]. Following the same logic applied to the continuous regime, the quasimomenta k_j turn out to be of the same form as in Eq. (15), which when plugged into the energy $E = -2 \sum_j \cos k_j$ and subsequently differentiating with the flux gives us

$$I(\phi) = -\frac{2\pi}{N_s} E_m \sin \left[\frac{2\pi}{N_s} \left(D + \frac{X}{N_p} + \phi \right) \right], \quad (18)$$

where $E_m = 2 \sin(\frac{N_p \pi}{L}) / \sin(\frac{\pi}{L})$ and $D = \frac{I_{max} + I_{min}}{2}$ [37, 70][71]. Naturally, for a fixed number of particles and increasing lattice sites in the system, Eq. (18) tends to Eq. (17).

III. ANALYSIS OF THE DENSITY AT THE SITE OF THE LOCALIZED IMPURITY

In this section, we assess the influence of the impurity, whether it's strengthened or weakened, by looking at the density on the site where it is residing, denoted by n_{imp} .

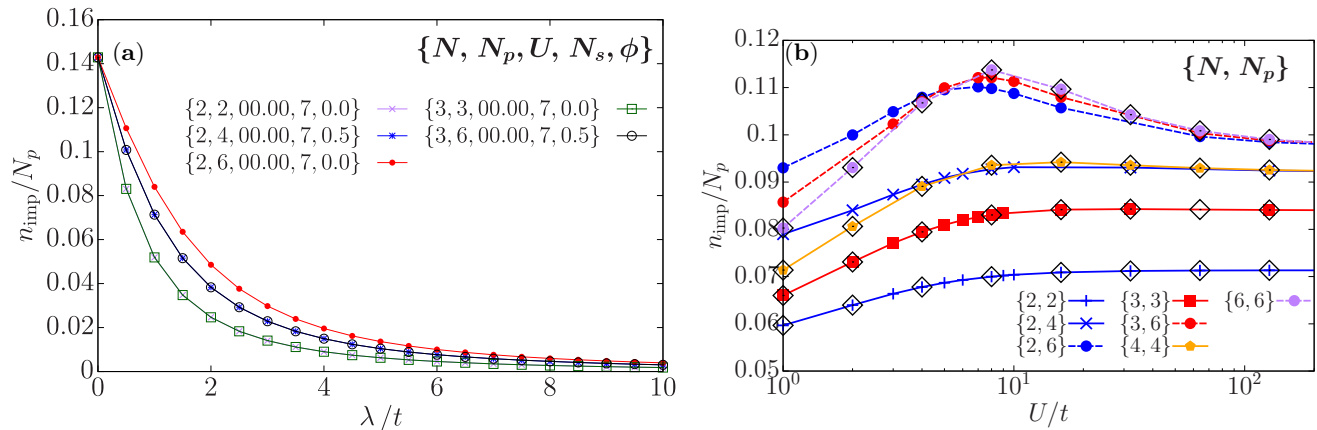


FIG. 4. *Density at the site of the impurity dependence on the interplay between barrier strength and interaction.* (a) Figure depicts the density at the barrier n_{imp} normalized by the number of particles N_p in a ring composed of N_s sites for non-interacting fermions as a function of the barrier strength λ in the absence of flux ϕ and different number of components N . (b) n_{imp} for fixed $\lambda/t = 1$ as a function of U/t for different N_p and N at $\phi = 0$. Grey triangles correspond to single-component bosons with the same N_p . Results obtained with exact diagonalization of the $SU(N)$ Hubbard and Bose-Hubbard model. *Note: The cases with even N_p/N are recorded at $\phi/\phi_0 = 0.5$ due to a parity effect.*

For free fermions at zero flux and zero barrier strength λ , the normalized density n_{imp} for different cases of number of components N and particles N_p is uniform throughout with a density of $1/N_s$. On increasing λ , n_{imp} displays a monotonic behaviour as the role of the static impurity is to halt the flow of particles. Several interesting trends appear in Fig. 4(a). Firstly, cases with the same N_p/N coincide with one another. Secondly, the barrier exerts its influence more on decreasing N_p/N , i.e. going to larger N . At zero interactions, one can picture the system with N components as N rings that are essentially free from one another. As a result, each ring will pay an energy penalty of λ amounting to a total contribution of $N\lambda$, enticing the particles to avoid the barrier more. Therefore, for a fixed particle number, the barrier will be more effective upon increasing N . An alternative way of seeing this is that the number of particles that can reside at the impurity site is limited by the Pauli exclusion principle thereby limiting the barrier's impact.

Switching on interactions, the density profile at the impurity site is monotonic for systems where $N_s \gg N_p$ – Fig. 4(b). Going to weak interactions, the barrier is screened due to the repulsion between the particles. The n_{imp} at equal N_p/N split and for a given N_s re-arrange themselves with increasing N_p displaying a further ordering dictated by N , still observing the trend of the impurity being weakened for larger N_p/N . However, we remark that since the interactions are effectively enhanced with N , the rate at which the barrier is suppressed increases with N and for fixed

number of components is governed by N_p –Fig. 5(c). Indeed, the rate grows approaching $N_p/N = 1$ corresponding to a “bosonic” limit. Consequently, there are crossings between the curves of n_{imp} with the most notable being for fixed N_p and various N reversing the trend of N_p/N present in the non-interacting regime –Fig. 4(b). Pushing interactions even further as $U \rightarrow \infty$, the distinction between N is disregarded due to forming a collective state comprised of a stiff particle arrangement arising from the spin correlations.

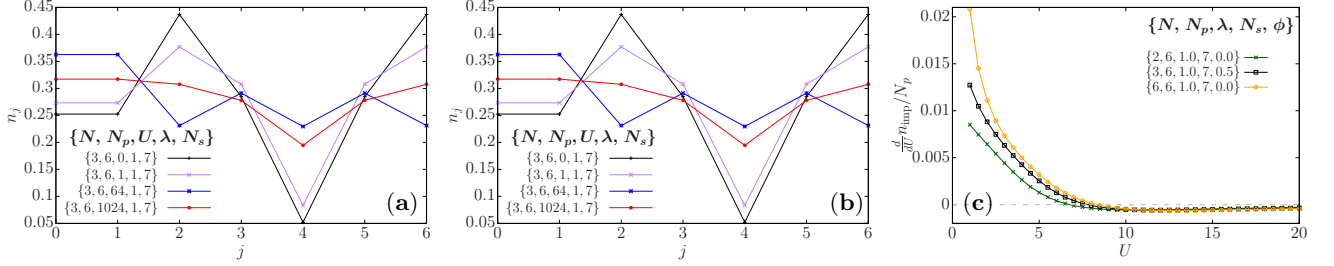


FIG. 5. *Density at each site of the ring for various interactions.* Figure showcases the density n_j at each site of the ring of N_s sites with fixed barrier strength λ/t and various interactions U/t in the absence of flux for $N_p = 6$ particles with different number of components (a) $N = 2$ and (b) $N = 3$. The global minimum is located on the site of the impurity at $N_s = 4$. (c) Rate of change of density with interaction denoted by $\frac{d}{dU} n_{\text{imp}}$. Results obtained with exact diagonalization of the $SU(N)$ Hubbard model.

In the cases where N_s is comparable to N_p , n_{imp} displays a non-monotonous behaviour originating as a finite size effect –Fig. 5(c). In order for the fermions to minimize the increased repulsion between them, they occupy the impurity site where the barrier essentially acts as a shield, since in this regime the particle occupation per site becomes restricted. Once again, the rate at which the barrier is augmented is faster with N due to the enhanced effective repulsion. For larger system sizes, the non-monotonicity is no longer there as depicted in Fig. 6.

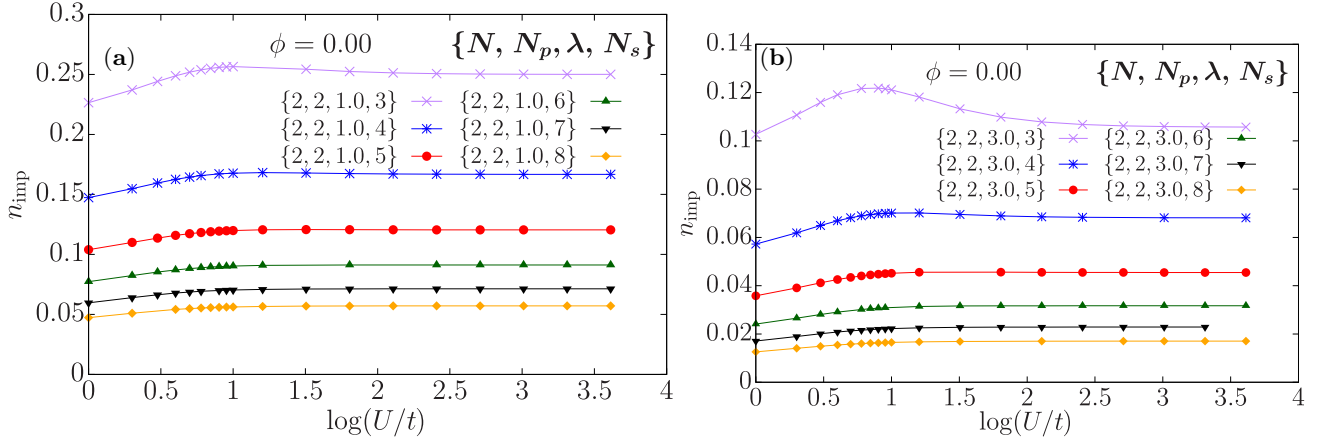


FIG. 6. *Density at the site of the impurity as a function of the number of sites and interaction.* Figure depicts the density at the barrier n_{imp} as a function of the interaction U/t with increasing lattice sites N_s for a fixed barrier strength $\lambda/t = 1$ and $\lambda/t = 3$ in panels (a) and (b) respectively in the absence of flux ϕ . Results obtained with exact diagonalization of the $SU(N)$ Hubbard.

A very interesting feature emerges in the density when subjected to an effective magnetic flux ϕ in the presence of a barrier. Specifically, the profile of n_{imp} becomes periodic with ϕ reflecting the period of the energy and persistent current, which is given by the bare flux quantum ϕ_0 in the free fermion regime and the fractional flux quantum ϕ_0/N_p observed at strong interactions –Fig. 7. As the current in the system grows larger, corresponding to a bigger particle flow, the impact of the barrier is enhanced reaching a maximum at the ϕ , where the energy level crossing occurs, in the absence of the impurity. Subsequently, a reduction in current is portrayed by a weakened impact of the barrier. Through this, we observe that the barrier captures the periodic nature of the current and provides an alternative route to monitor fractionalization.

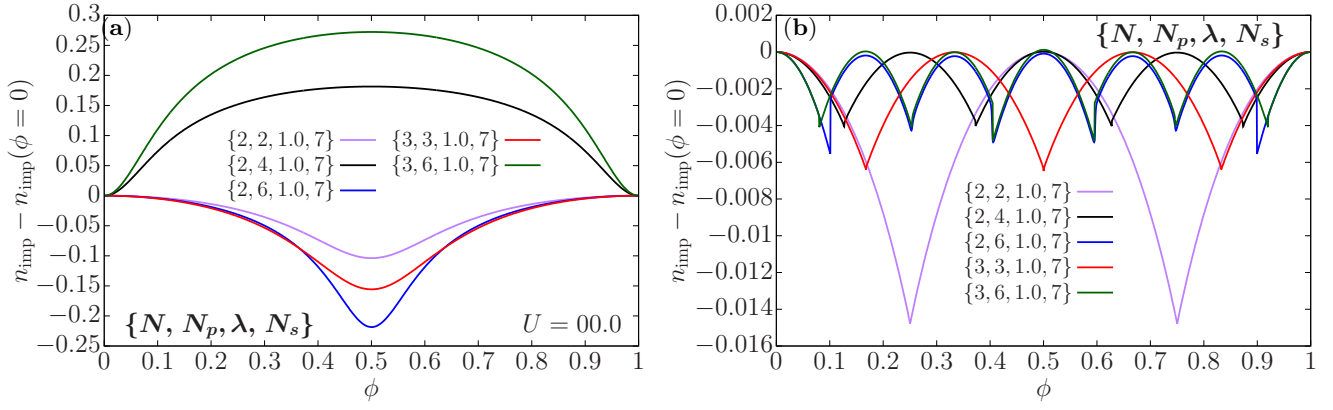


FIG. 7. *Density at the site of the impurity as a function of the flux.* Depiction of the density at the barrier site n_{imp} for fixed barrier strength $\lambda/t = 1$ as a function of the flux ϕ for different number of particles N_p and components N at interactions (a) $U/t = 0$ and (b) $U/t = 1024$. Results obtained with exact diagonalization of the $SU(N)$ Hubbard.

IV. $SU(N)$ FERMIONIC PERSISTENT CURRENTS IN A SYSTEM WITH A LOCALIZED IMPURITY

The second probe utilized in our analysis is the persistent current $I(\phi)$. Firstly, we start by remarking that in the non-interacting regime the periodicity of the current as a function of the flux, with a period fixed by ϕ_0 originates from energy level crossings between parabolas of different angular momenta. This occurs to counteract the flux and minimize the energy of the system. In the case of fermions, these degeneracy points depend on their population parity occurring at $\phi = (2n + 1)/2$ or $\phi = n$ when the number of particles $N_p = (2m + 1)/N$ and $N_p = (2m)N$ prompting a diamagnetic and paramagnetic response, respectively. In the presence of a barrier and zero interactions, the opening of the spectral gap at these degeneracy points smears the characteristic saw-tooth shape of the current eventually turning into a sinusoid shape as the barrier strength λ becomes sufficiently large –Fig. 8(a). Additionally, the magnitude of the current decreases with increasing λ as is expected.

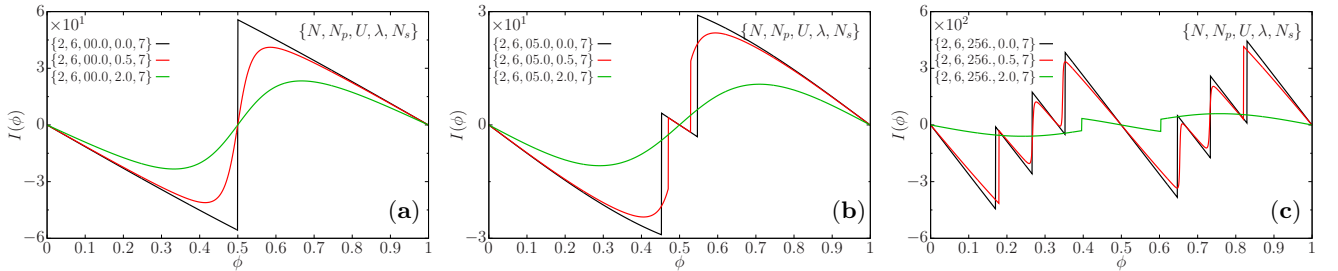


FIG. 8. *Persistent current against flux for a fixed interaction.* Figure shows the persistent current $I(\phi)$ as a function of the flux ϕ for different barrier strengths λ at fixed interactions (a) $U/t = 0$, (b) $U/t = 1$ and (c) $U/t = 10$. Results obtained with exact diagonalization of the $SU(N)$ Hubbard model for $N_p = 2$ particles with $SU(2)$ symmetry in a ring of $N_s = 7$ sites.

In the absence of a barrier, strongly interacting fermionic matter-wave currents undergo fractionalization stemming from the spin correlations in the system resulting in them having a reduced period, which depends on whether the system has repulsive or attractive interactions [38]. For the repulsive case under consideration here, N_p piece-wise parabolic segments appear in the energy spectrum per flux quantum reflecting the fractional values of the angular momentum per particle. On account of this phenomenon, there is an intriguing interplay between the interaction and the impurity. Specifically, the profile of the current becomes hybridized showcasing both smoothening and fractionalization –Figs. 8 and 9. Such a behaviour is similar to the profile of matter-wave currents observed in the extended $SU(N)$ Hubbard model in the commensurate regime of one particle per site [72]. Eventually as $U \rightarrow \infty$, the effect of the barrier is significantly diminished and the current exhibits the characteristic $1/N_p$ periodicity. However, we note that while the value of the persistent current saturates to a value close to that obtained through Bethe Ansatz in the absence of a barrier, it does not coincide exactly.

To properly visualize the interplay between interaction and impurity, we resort to plotting the maximum current

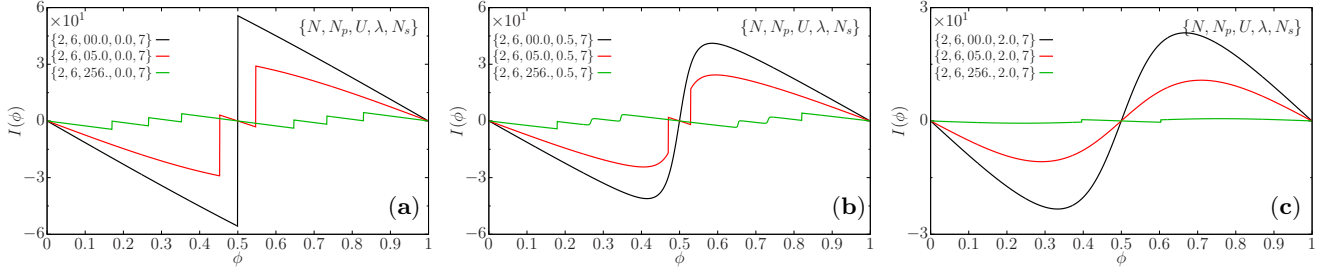


FIG. 9. *Persistent current against flux for a fixed barrier.* Figure illustrates the persistent current $I(\phi)$ as a function of the flux ϕ for different interactions U/t at fixed barrier strength (a) $\lambda/t = 0$, (b) $\lambda/t = 1$ and (c) $\lambda/t = 10$. Results obtained with exact diagonalization of the $SU(N)$ Hubbard model for $N_p = 2$ particles with $SU(2)$ symmetry in a ring of $N_s = 7$ sites.

amplitude I_{\max} that displays a non-monotonic behaviour –Fig. 10(a) and (b). Firstly, we point out that I_{\max} at zero barrier and interactions is larger on increasing N_p and for fixed particle number is greater on going to $N_p/N = 1$ [51]. At weak U and a given λ , the barrier is suppressed for the same reason presented in Sec. III at rate that firstly depends on N and then on N_p . From Fig. 10(c), it is clear that the barrier is screened out faster for larger N due to the increased effective repulsion up to NU arising from the loosened Pauli exclusion principle. We emphasize that the fractionalization does not play a role as the gaps that open up inhibit energy level crossings, which will now occur at a larger value of interaction compared to the one in the absence of a barrier. Indeed, this is evidenced by the currents for $N_p/N = 1$ and that of bosons with same N_p coinciding in this regime –Fig. 10(a). For single-component bosons subjected to repulsive interactions there is no such phenomenon of fractionalization.

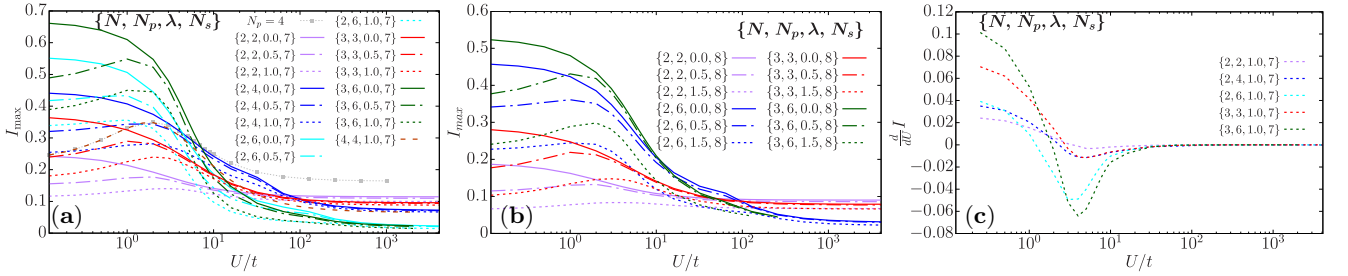


FIG. 10. *Persistent current behavior dependence on the interplay between interaction and impurity.* Persistent current amplitude I_{\max} as a function of the interaction U/t for different barrier strengths λ/t , number of particles N_p and number of components N in a ring of (a) $N_s = 7$ and (b) $N_s = 8$ sites. (c) Rate of change of the current $\frac{d}{dU} I_{\max}$ with interactions for fixed barrier strength. Results obtained with exact diagonalization of the $SU(N)$ Hubbard.

At the bump corresponding to intermediate U , we observe that I_{\max} of the bosons and corresponding fermionic case with $N_p/N = 1$ start to separate indicating with the amplitude of the latter system being more reduced. Such behaviour indicates that the fractionalization is now playing a key role with the impact of the barrier being severely diminished. There are three indicators in this regard: (i) for $\lambda = 0$ fractionalization decreases the current magnitude –Fig. 10(a) and (b); (ii) cases with same N_p but different N overlap reflecting the $1/N_p$ periodicity as $U \rightarrow \infty$; (iii) values of the current approach those calculated from Bethe Ansatz from Eq. (18). Lastly, the trend observed in the weakly interacting regime of I_{\max} growing with N_p is now reversed.

In addition to the phenomenon of fractionalization, the current magnitude is decreased due to strong quantum phase fluctuations. Seeing as for strong interactions the system is in a collective state of a stiff particle arrangement, there are no density fluctuations, hence prompting ones in the phase. Such is the case for repulsive bosons [35]. To understand this better, we can consider the quantum phase model \mathcal{H}_{QPM} , which the Bose-Hubbard Hamiltonian maps to in the limit $\bar{n} = N_p/N_s \gg 1$ [73]. By writing the annihilation operator in the Bose-Hubbard model as $a_j \sim \sqrt{\bar{n}} e^{i\varphi_j}$, we have that

$$\mathcal{H}_{QPM} = -2J \sum_{\langle i,j \rangle} \cos(\varphi_i - \varphi_j) + \frac{U}{2} \sum_i \delta n_i^2, \quad (19)$$

where φ_i and δn_j are conjugate operators for the phase and density fluctuations respectively with $[\varphi_i, \delta n_j] = i\hbar \delta_{ij}$. The parameters $J = t\bar{n}$ and $\delta n_j = \bar{n} - n_j$ correspond to the Josephson coupling and density fluctuations. From

here, it becomes clear that as the interactions increase the number fluctuations on the site become smaller compared to those of the phase as otherwise the energy would increase. Furthermore, we note that quantum phase model is used to describe the physics of the Josephson junction, which is essentially the tunneling of particles through a barrier.

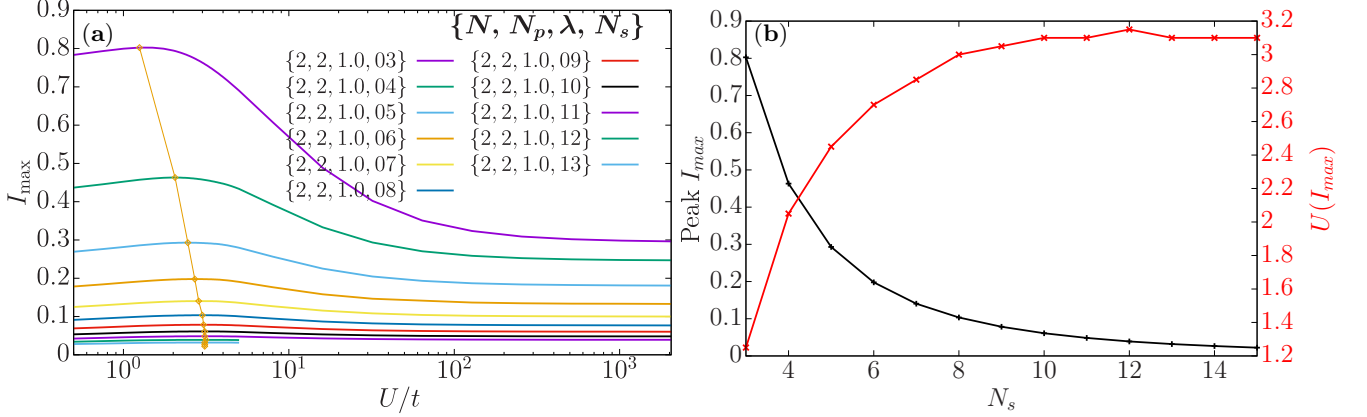


FIG. 11. *Optimal persistent current dependence on increasing system size.* (a) Figure illustrates the changes in the peak of the current amplitude I_{\max} on increasing the number of sites in the ring N_s as a function of the interaction U/t for $N_p = 2$ particles with SU(2) symmetry and fixed barrier strength λ/t . orange line acts as a guide to the eye. (b) Change in the magnitude peak of I_{\max} (black) and the interaction at which it is obtained (red) as a function of N_s . Results obtained with exact diagonalization of the SU(N) Hubbard.

To conclude, we remark that the optimal current as a function of U and λ , corresponding to the peak of I_{\max} , decreases as a function of the number of sites N_s . Naturally, this is to be expected as the current is a mesoscopic effect with a $1/N_s$ dependence as shown by Eq. 18. On the other hand, the interaction at which this optimal current is obtained, grows with N_s until it saturates at large N_s . This saturation can be understood from the density where the barrier is suppressed with interaction monotonously when N_s is larger than N_p .

V. ANALYSIS OF THE SPECTRAL GAP

Typically, the introduction of a static impurity opens a gap Δ at all degeneracy points in the spectrum. Such is the case for single-component bosons with repulsive and attractive interactions, as well as for spinless fermions. When considering SU(N) fermions, a condition is imposed for a gap to appear: the effective total spin, computed through the quadratic Casimir, corresponding to the intersecting parabolas needs to be the same to have the avoided level crossings.

The total quadratic Casimir operator is defined as

$$C_{1,\text{tot}} = \left(\sum_i \vec{S}_i \right)^2 = \sum_i \vec{S}_i^2 + 2 \sum_{i \neq j} \vec{S}_i \cdot \vec{S}_j, \quad (20)$$

where $\vec{S}_i := \frac{1}{2} c_{i,\alpha}^\dagger \vec{\sigma}_{i,\alpha,\beta} c_{i,\beta}$ using the Einstein sum convention and $\vec{\sigma}_i$ are the SU(N) extensions of the Pauli matrices. On a given site i , we have that

$$\vec{S}_i^2 = \frac{N-1}{2N} \sum_{\alpha} n_{i,\alpha} \left(1 - \sum_{\beta} n_{i,\beta} \right), \quad (21)$$

which turns out to be a function of number operators. In our setting, the static impurity is provided solely through the local density $\mathcal{H}_{\text{imp}} = \sum_{\alpha} \lambda_{\alpha} n_{0,\alpha}$ where λ_{α} is the impurity strength for species α and n_0 is the number operator denoting that the impurity is located on site 0. It is clear that impurity Hamiltonian commutes with \vec{S}_i^2 since both of them contain just number operators. We are left with calculating $[\sum_{i \neq j} \vec{S}_i \cdot \vec{S}_j, \sum_{\alpha} \lambda_{\alpha} n_{0,\alpha}]$, which results to be

$$\left[\sum_{i \neq j} \vec{S}_i \cdot \vec{S}_j, \sum_{\alpha} \lambda_{\alpha} n_{0,\alpha} \right] = \sum_{\epsilon} \sum_{j \neq 0} \sum_{\alpha, \beta, \gamma} \sigma_{0;\alpha,\beta}^{\epsilon} \sigma_{j;\beta,\gamma}^{\epsilon} c_{j,\beta}^{\dagger} c_{j,\gamma} c_{0,\alpha}^{\dagger} c_{0,\beta} (\lambda_{\beta} - \lambda_{\alpha}). \quad (22)$$

Hence, the commutator is equal to zero *iff* the impurity's strength is independent of the species. Otherwise, if it is not, the $SU(N)$ symmetry is broken explicitly. Considering the conditions of Ref. [57], where an equal number of particles per species N_α is chosen, the calculation of the quadratic Casimir simplifies to

$$C_{1,\text{tot}} = \sum_{\alpha} S_{\text{tot}}^{\alpha} S_{\text{tot}}^{\alpha} = \sum_{\alpha=1}^{N(N-1)} (S_{xy;\text{tot}}^{\alpha})^2 + \sum_{\gamma=1}^{N-1} (S_{C;\text{tot}}^{\gamma})^2, \quad (23)$$

where $S_{C;\text{tot}}^{\gamma}$ symbolizes the $N - 1$ diagonal Cartan elements of the generators and $S_{xy;\text{tot}}^{\alpha}$ the remaining part. Since $S_{C;\text{tot}}^{\gamma}$ gives zero weight for the states that we consider, the quadratic Casimir reduces to

$$C_{1,\text{tot}} = \sum_{\alpha=1}^{N(N-1)} (S_{xy;\text{tot}}^{\alpha})^2. \quad (24)$$

Since the barrier commutes with the quadratic Casimir operator in the cases under our consideration of species-independent λ , then it can only couple states *iff* the corresponding eigenstates share the same Casimir value[74]. Whilst at zero interaction, all energy level crossings in the ground-state have the same Casimir value, which is marked by the smoothing of the current, the same cannot be said on going to stronger U . On account of fractionalization, mediated by various energy level crossings from the spin correlations, the N_p piece-wise parabolas are characterized by different Casimir values especially on going to larger $SU(N)$ resulting in selective gap openings –Fig. 12.

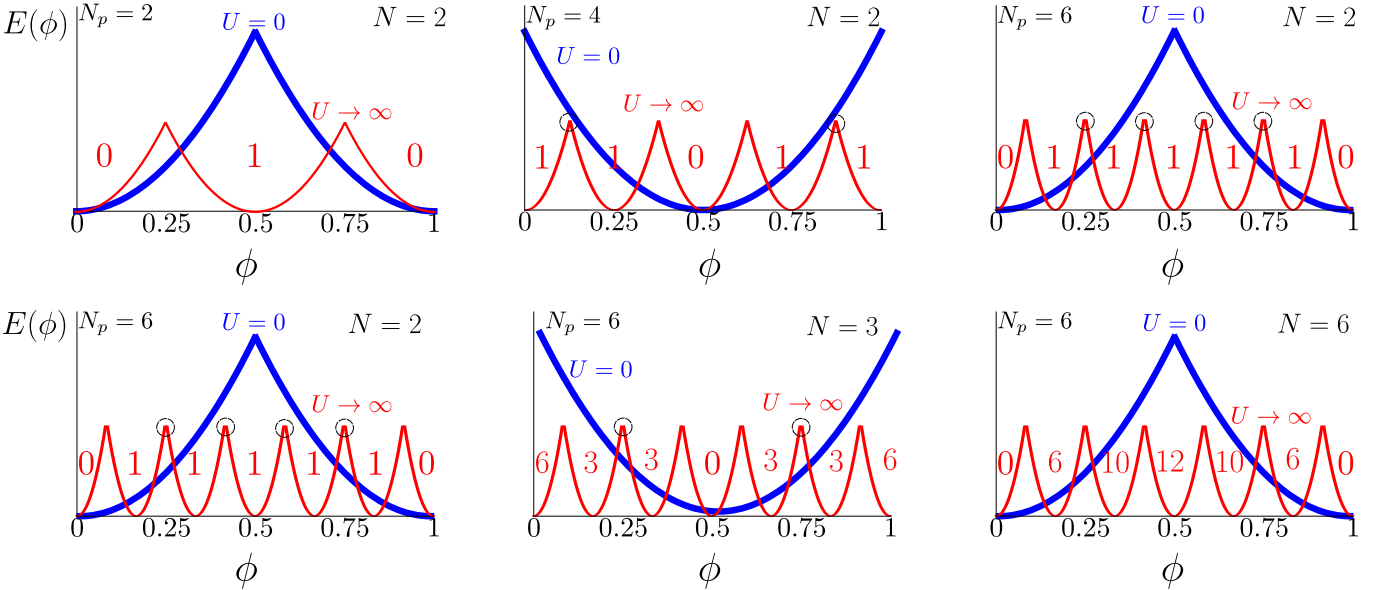


FIG. 12. schematic figure for the energy landscape $E(\phi)$ as a function of the effective magnetic flux at interactions $U/t = 0$ and $U/t \rightarrow \infty$ for N_p particles and N components. The numbers in each parabolas correspond to the Casimir value associated to it with the black dotted circles indicating where a gap opens up.

Fixing the barrier and going to weak interactions, we have that the gap opening depends on the parity and the number of components whereby the system can behave in two ways. For *diamagnetic parity and odd N* , the energy level crossings due to fractionalization intersect each other at $\phi = 0.5$ [51], such that the adjacent parabola have the same Casimir values opening a spectral gap. It turns out, that such behaviour is an exception as in all other cases[75] the spectral gap remains closed at all intersection points, at difference with the bosonic counterpart. Consequently, the spectral gap observed in the free-particle regime is now pushed towards highly excited states as there are no adjacent parabolas with the same Casimir representation. Nonetheless, we point out that this gap still produces some deformation of the energy parabolas and a weak smoothing of the current.

Ramping up to stronger interactions, more parabolas descend to the ground-state due to fractionalization to given N_p energy level crossings. Consequently, there are more gaps that can be opened if the condition of having the same Casimir value is met. For a given number of particles and different component number, we find that the number of gap openings and their subsequent flux dependence, i.e. which degeneracy point is split, varies. Specifically, we

remark that for fixed N_p the number of spectral gaps present decreases on going to larger N and is zero at $N_p/N = 1$ since the number of Casimir values the parabolas can adopt grows with N .

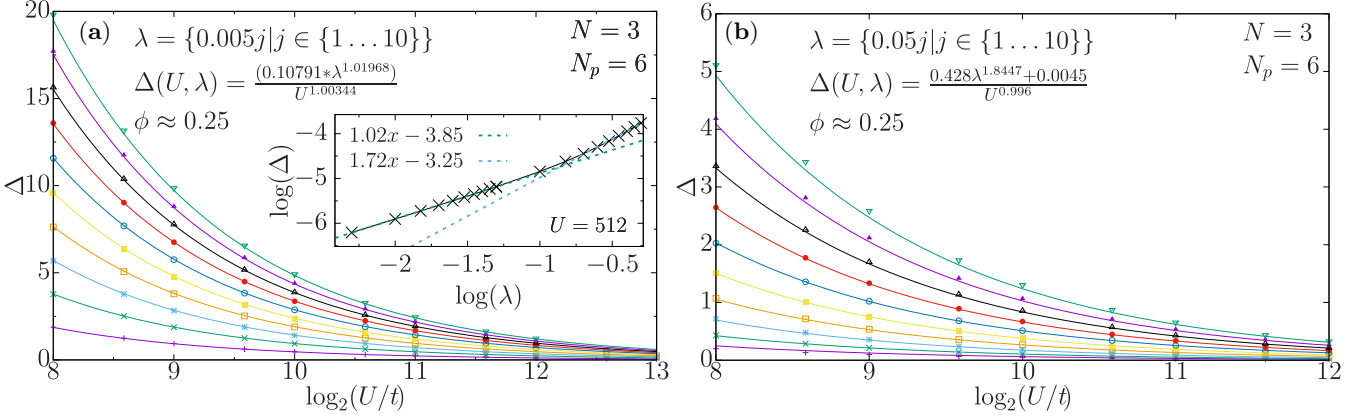


FIG. 13. *Spectral gap behaviour as a function of barrier strength and interaction.* Figures show the gap Δ , at flux $\phi \approx 0.25$ that would correspond to the crossing between parabolas two and three in the ground-state energy landscape, as a function of interaction U/t for $N_p = 6$ particles with SU(3) symmetry at (a) weak and (b) strong barrier strengths. Inset panel shows the gap versus lambda and interaction fixed to a value $U/t = 512$ in a log-log plot. Two dotted lines show the different behavior as function of λ/t and U/t . Results obtained with exact diagonalization of the SU(N) Hubbard model with $N_s = 7$ sites. Note that the system is at a sufficiently strong interaction such that N_p peaks are already present in the ground-state.

The scaling of the gap Δ as a function of the interaction is monotonically decreasing –Fig. 13. To understand the scaling behaviour, we consider the exact Bethe Ansatz equations in the infinitely repulsive limit following the works [57, 60]. In this regime, it was shown that there is a spin-charge decoupling of the Bethe equations such that the system can be described as a composition function of the spinless and SU(N) Heisenberg model, accounting for the charge and spin parts of the system respectively. The energy contribution from the spin-part scales with $1/U$, leading to a full degeneracy of the spin part at $U \rightarrow \infty$ where all the gaps close. For weak barrier strengths the scaling is linear as $\Delta(U, \lambda) \approx \lambda/U$ (see Fig. 13(a)), compatible with a perturbative expansion in low-energy descriptions, whilst for stronger ones it becomes non-linear $\Delta(U, \lambda) \approx \lambda^\xi/U$ (see Fig. 13(b)).

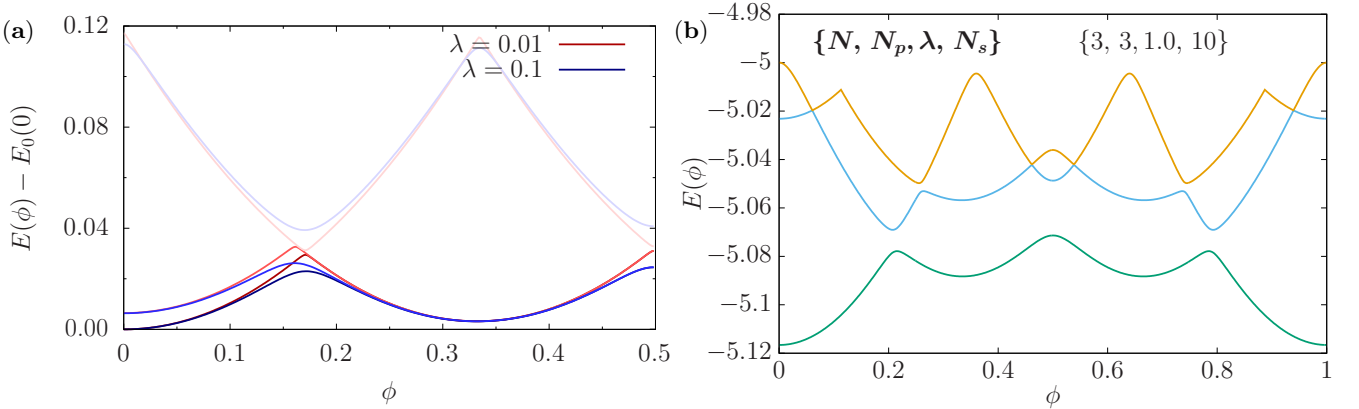


FIG. 14. *Spectral gap opening for SU(N) symmetry breaking.* (a) Energy $E(\phi)$ versus flux ϕ with a fixed interaction $U/t = 256$ and different barrier strengths (acting only on one species) λ/t . For any value of the λ/t a gap opens up. (b) $E(\phi)$ against ϕ for fixed $\lambda/t = 1$ where the SU(3) symmetry is broken by choosing different interactions between the components $U_A/t = 10$, $U_B/t = 20$ and $U_C/t = 30$. Results obtained with exact diagonalization of the SU(N) Hubbard model for $N_p = 3$ three-component fermions residing in a ring of $N_s = 10$ sites.

To conclude, we note that by choosing a colour selective barrier, e.g. only applying a barrier for one colour, a gap opens for very small values of the barrier strength λ . Furthermore, gaps are present everywhere in the ground-state compared to the isotropic barrier case –Fig. 14(a). Similarly, breaking the SU(3) symmetry explicitly by choosing a species-dependent interaction lifts degeneracies opening some of the previously closed gaps –Fig. 14(b). Note that this method of breaking the SU(N) symmetry is only possible for $N > 2$.